Bull. Mater. Sci. (2019) 42:163
https://doi.org/10.1007/s12034-019-1859-4

Influence of Ni doping on the structural, ferroelectric, magnetic and optical properties of $Bi_{0.85}Nd_{0.15}Fe_{1-x}Ni_xO_3$ thin films

HUA WANG*, DONG HAN, JIWEN XU and LING YANG
School of Materials Science and Engineering, Guilin University of Electronic Technology, Guilin 541004, People's Republic of China
*Author for correspondence (wh65@tom.com)

MS received 9 September 2018; accepted 29 January 2019; published online 21 May 2019

Abstract. $Bi_{0.85}Nd_{0.15}Fe_{1-x}Ni_xO_3$ ($x = 0.025$–0.125) thin films were synthesized by applying a sol–gel method on fluorine-doped tin oxide substrates. The influence of Ni doping concentration on the structure, leakage current, ferroelectric, magnetic and optical properties of $Bi_{0.85}Nd_{0.15}Fe_{1-x}Ni_xO_3$ thin films was investigated. $Bi_{0.85}Nd_{0.15}Fe_{1-x}Ni_xO_3$ thin films are polycrystalline films that present a single perovskite structure without any impurity phase when the Ni doping concentration is below 0.1 and present a $Bi_2Fe_4O_9$ phase when the Ni doping concentration is above 0.1. The grain size of the films and their holes gradually decrease with an increase in the Ni doping amount. The saturation magnetization of $Bi_{0.85}Nd_{0.15}Fe_{1-x}Ni_xO_3$ thin films increases with Ni content. However, appropriate Ni doping concentration can decrease the leakage current and enhance the ferroelectric polarization and optical transmittance of the films. Meanwhile, the absorption edge has a slight red shift. $Bi_{0.85}Nd_{0.15}Fe_{1-x}Ni_xO_3$ thin films possess better combination properties at a leakage current density of 4.27×10^{-9} A cm^{-2}, ferroelectric polarization of 28.58 μC cm^{-2}, saturation magnetization of 2.08 emu cm^{-3} and transmittance of over 85% when the Ni doping concentration, x is 0.05.

Keywords. $Bi_{0.85}Nd_{0.15}Fe_{1-x}Ni_xO_3$; Ni-doping; thin film; ferroelectric property; leakage current.

1. Introduction

Multiferroic materials, which possess ferroelectric, ferromagnetic and ferroelastic characteristics within a single phase, are widely used in data storage, sensors and spintronic devices. Among all the identified single-phase multiferroic materials, $BiFeO_3$ (BFO) exhibits a large spontaneous polarization value, high ferroelectric Curie temperature ($T_C = 830$°C) and anti-ferromagnetic Neel temperature ($T_N = 370$°C) [1–8]. However, serious disadvantages, such as the large leakage current and the weak ferromagnetic properties, still need to be overcome in the BFO thin films.

The site-engineering concept has been widely explored in an effort to enhance the ferroelectric or ferromagnetic properties of BFO. There are many reports on the doping of lanthanoid atoms (Nd, La, Ho, Nb, etc.) at Bi-sites in BFO with the enhanced ferroelectric properties [9–12]. A lot of studies also reported that the doping of transition metal ions (Co, Mn, Zn, etc.) at Fe sites could enhance the magnetoelectric properties of BFO [13–15]. However, it is difficult to reduce the leakage current density of BFO thin films by introducing the single ion [16]. Moreover, sometimes, the single ion doping shows weakness in terms of improving the ferroelectric properties or the ferromagnetic properties. Recently, considerable research studies have reported that co-doped Bi sites and Fe sites are effective in obtaining large remnant polarization and low leakage current density. Raghavan *et al* [17] increased the ferroelectric properties and reduced the leakage current density in (Nd, Cu) co-doped BFO thin films prepared by employing a chemical solution deposition method. Zhang *et al* [18] enhanced the ferroelectric properties of (Nd, Co) co-doped BFO thin film compared with a single-doped sample.

In this work, Nd and Ni co-doped $Bi_{0.85}Nd_{0.15}Fe_{1-x}Ni_xO_3$ ($x = 0.025$, 0.050, 0.075, 0.100 and 0.125) thin films are prepared by using the sol–gel method on fluorine-doped tin oxide (FTO) substrates for the potential application in transparent electronics. The influences of Ni doping concentration on the structure, leakage current, ferroelectric, magnetic and optical properties of $Bi_{0.85}Nd_{0.15}Fe_{1-x}Ni_xO_3$ are investigated.

2. Experimental

$Bi_{0.85}Nd_{0.15}Fe_{1-x}Ni_xO_3$ thin films were prepared through the sol–gel method, and transparent conductive FTO/glass was utilised as the substrate. For the preparation of precursor solutions of $Bi_{0.85}Nd_{0.15}Fe_{1-x}Ni_xO_3$ films, $Bi(NO_3)_3 \cdot 5H_2O$, $Fe(NO_3)_3 \cdot 9H_2O$, $Nd(NO_3)_3 \cdot 6H_2O$ and $Ni(NO_3)_3 \cdot 6H_2O$ were dissolved in 2-methoxyethanol and acetic anhydride (4:1 in volume) based on the compound stoichiometric ratios. After stirring the solutions for 5 h, the final solution concentration was determined to be 0.3 M. All the reactions were performed at room temperature.

$Bi_{0.85}Nd_{0.15}Fe_{1-x}Ni_xO_3$ thin films were spin-coated on an FTO/glass substrate with a rotation speed of 4000 rpm for 20 s. The wet $Bi_{0.85}Nd_{0.15}Fe_{1-x}Ni_xO_3$ thin films were baked on a heating plate for 5 min at 200°C and annealed by using a rapid thermal processor system at 400°C for 10 min. The final annealing procedure was performed at 550°C for 20 min. The above process was repeated several times until the desired film thickness was obtained. Circular Au top electrodes with a diameter of 0.4 mm were deposited through electron beam evaporation and with a shadow mask. Good contact between the electrodes and films was ensured by applying a post annealing procedure at 300°C for 20 min.

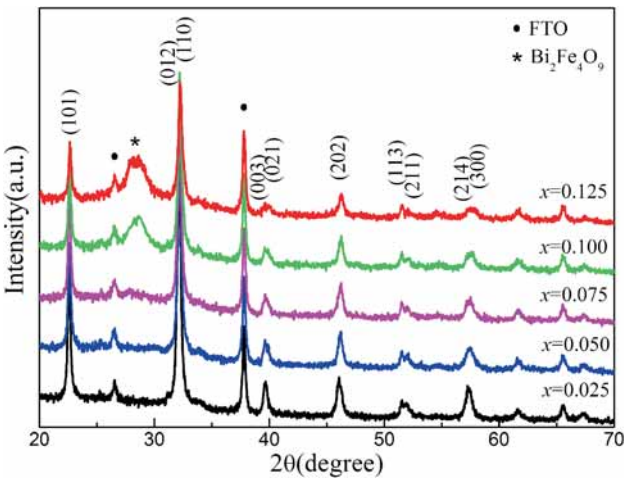

Figure 1. XRD patterns of $Bi_{0.85}Nd_{0.15}Fe_{1-x}Ni_xO_3$ thin films.

The crystal and phase structures of $Bi_{0.85}Nd_{0.15}Fe_{1-x}Ni_xO_3$ films were analysed through X-ray diffraction (XRD; D8-Advance, Bruker). The surface morphology of the films was observed by field emission scanning electron microscopy (SEM; S4800, Toshiba). The leakage current density, ferroelectric, magnetic and optical properties of the films were measured with a digital source meter (2400, Keithley), ferroelectric analyser (P-PMF, Radiant), vibrating sample magnetometer (Microsense EZ9) and UV–Vis spectrophotometer (UV-6100, China), respectively.

3. Results and discussion

Figure 1 shows the XRD patterns of $Bi_{0.85}Nd_{0.15}Fe_{1-x}Ni_xO_3$ thin films with different Ni doping concentrations. $Bi_{0.85}Nd_{0.15}Fe_{1-x}Ni_xO_3$ thin films are polycrystalline films with a single perovskite structure without any prominent impurity peaks when the Ni doping concentration is below 0.1. Apart from the relatively strong diffraction peaks of (101), (012) and (110), several relatively weak diffraction peaks, such as

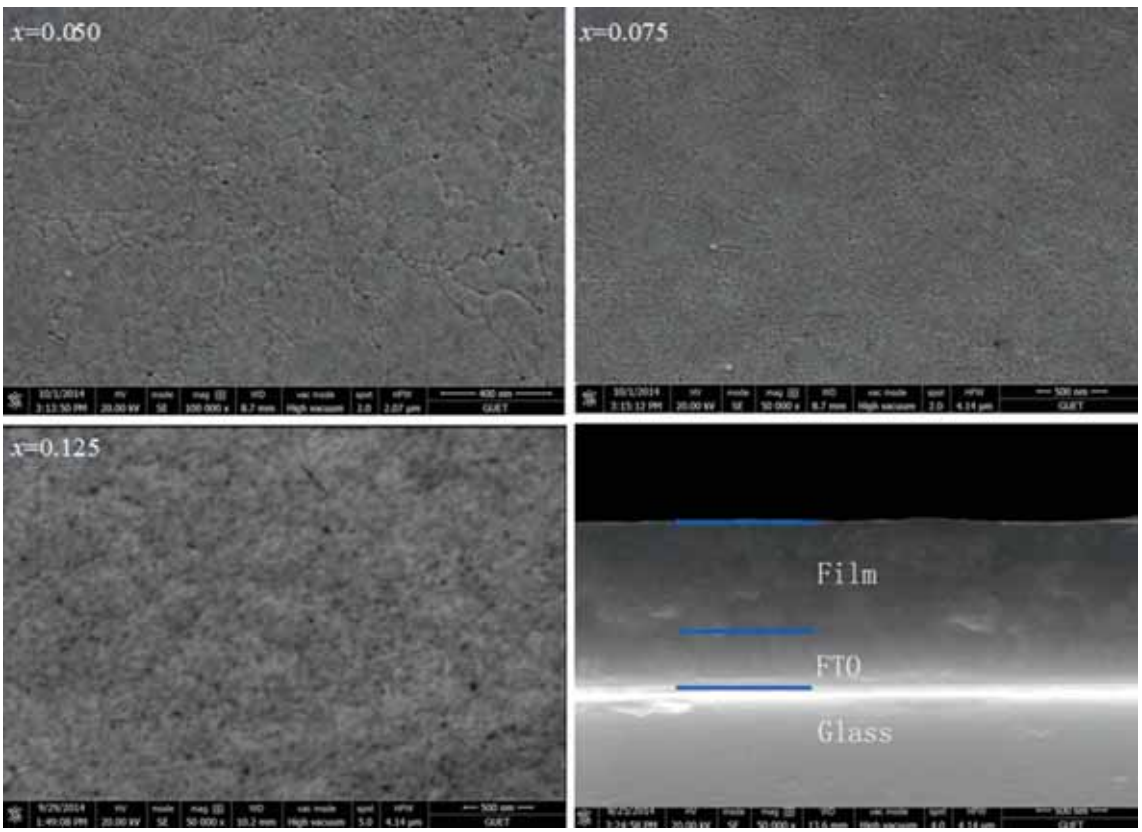

Figure 2. Surface and cross-sectional SEM images of $Bi_{0.85}Nd_{0.15}Fe_{1-x}Ni_xO_3$ thin films.

Table 1. Average grain size of the films estimated from SEM and calculated from XRD.

Ni doping amount	0.025	0.050	0.075	0.100	0.125
Estimated from SEM (nm)	80	70	66	63	60
Calculated from XRD (nm)	50	45	42	40	37

(021), (202), (113) and (300) are observed, which indicate good crystallinity in the films. Furthermore, the intensity in the (012) diffraction peak gradually decreases and the diffraction peak of (110) is gradually strengthened with an increase in the Ni doping amount, which indicate that Nd and Ni ions replace Bi and Fe ions, respectively, enter the crystal lattice and change the original crystal structure [19]. However, an impurity phase of $Bi_2Fe_4O_9$ appears between 28° and 30° when the doping amount is 0.1 and $Bi_2Fe_4O_9$ has no effect on the ferroelectric properties of the films [10].

Figure 2 shows the SEM images of the surface and cross morphology for $Bi_{0.85}Nd_{0.15}Fe_{1-x}Ni_xO_3$ thin films with different Ni doping concentrations. As shown in the figure, the crystallinity of the films is good and the surface is smooth and dense. The grain size of the films is large and few holes are obtained in these films. The average grain size of the films estimated from SEM is shown in table 1, and the grain size of the films gradually decreases with an increase in the Ni doping amount, which is in accord with that calculated by the Debye–Scherrer formula from XRD. In addition, the holes in the films also gradually decrease with an increase in the Ni doping amount. A small black spot appears in the films when the doping amount of Ni is above 0.1, which is $Bi_2Fe_4O_9$ that produced during annealing. From the cross-section of the film, $Bi_{0.85}Nd_{0.15}Fe_{1-x}Ni_xO_3$ films, FTO films and glass substrates are stratified, and no mutual diffusion is observed. The layer of $Bi_{0.85}Nd_{0.15}Fe_{1-x}Ni_xO_3$ thin films is in tight contact with the layer without obvious interface.

Figure 3 shows the leakage current density of $Bi_{0.85}Nd_{0.15}Fe_{1-x}Ni_xO_3$ thin films with a structure of Au/$Bi_{0.85}Nd_{0.15}Fe_{1-x}Ni_xO_3$/FTO measured at room temperature. As shown in the figure, the leakage current density of the films is small. The leakage current densities of the films at an electric field strength of 300 kV cm^{-1} are 2.78×10^{-8}, 4.27×10^{-9}, 7.63×10^{-9}, 9.59×10^{-9} and 2.01×10^{-8} A cm^{-2} when the Ni doping concentrations are 0.025, 0.050, 0.075, 0.100 and 0.125, respectively. These results indicate that the leakage current density of $Bi_{0.85}Nd_{0.15}Fe_{1-x}Ni_xO_3$ thin films first decreases and then increases with an increase in the Ni doping concentration. The leakage current density of Nd and Ni co-doping BFO films is three orders of magnitude lower compared with undoped BFO thin films [8] and one order of magnitude lower than that of single Nd-doped BFO thin films [12]. Oxygen vacancies are the primary cause of leakage current, because of the mobility of Bi^{3+} or the transformation from Fe^{3+} to Fe^{2+} [20,21]. Nd and Ni co-doping remarkably

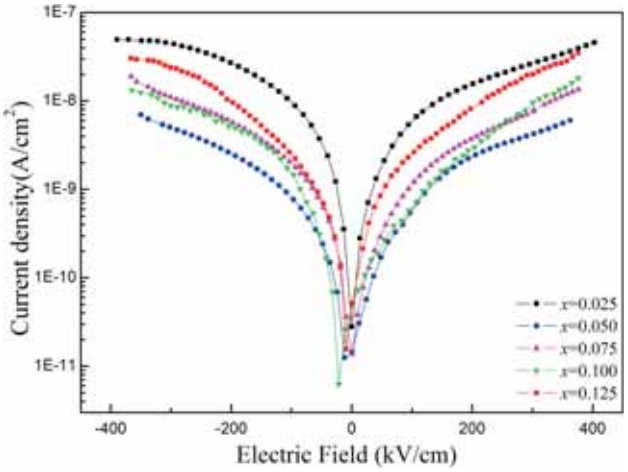

Figure 3. J–E curves of Au/$Bi_{0.85}Nd_{0.15}Fe_{1-x}Ni_xO_3$/FTO capacitors.

reduces the oxygen vacancy produced by the volatilization of Bi elements in the heat treatment process, inhibits the transition from Fe^{3+} to Fe^{2+}, improves the densification of the films and reduces the leakage current of the films. A similar phenomenon is observed in La and Ni co-doped BFO thin film samples, in which the modification in lattice parameters with a rhombohedrally distorted perovskite structure is considered because of reduced leakage current in the film [22].

Figure 4 shows the P–E hysteresis loops and remnant polarization P_r of Au/$Bi_{0.85}Nd_{0.15}Fe_{1-x}Ni_xO_3$/FTO capacitors measured at 1 kHz and at room temperature. As shown in the figure, the shape of the hysteresis loop shows a certain elliptical shape, which indicates that the films still possess a certain leakage current. However, well-shaped P–E hysteresis loops can be observed in $Bi_{0.85}Nd_{0.15}Fe_{1-x}Ni_xO_3$ thin films with a Ni doping concentration, x of 0.05, indicating the lowest leakage current in the film example, which is consistent with the leakage current density change curves as shown in figure 3. Remnant polarization P_r and corresponding coercive field intensity, E_c of $Bi_{0.85}Nd_{0.15}Fe_{1-x}Ni_xO_3$ thin films are 26.41, 28.58, 17.67, 14.05 and 13.27 μC cm^{-2} and 393, 276, 461, 572 and 466 kV cm^{-1} when $x = 0.025$, 0.050, 0.075, 0.100 and 0.125, respectively. The ferroelectric remnant polarization of $Bi_{0.85}Nd_{0.15}Fe_{1-x}Ni_xO_3$ thin films first increases and decreases with an increase of Ni doping concentration, x. The maximum polarization is obtained in the $Bi_{0.85}Nd_{0.15}Fe_{1-x}Ni_xO_3$ sample with the Ni doping amount x of 0.05, which is higher than that of single Nd-doped $Bi_{0.85}Nd_{0.15}FeO_3$ films [12]. In addition, the P–E hysteresis loops are asymmetric, which is mainly due to the asymmetrical space charge accumulation between the electrodes and the $Bi_{0.85}Nd_{0.15}Fe_{1-x}Ni_xO_3$ thin films, caused by the top electrode Au and the bottom electrode FTO, resulting in different offsets in the electric field directions. Similar phenomena were observed in PLZT ferroelectric thin films with a structure of Pt/PLZT/ITO [23].

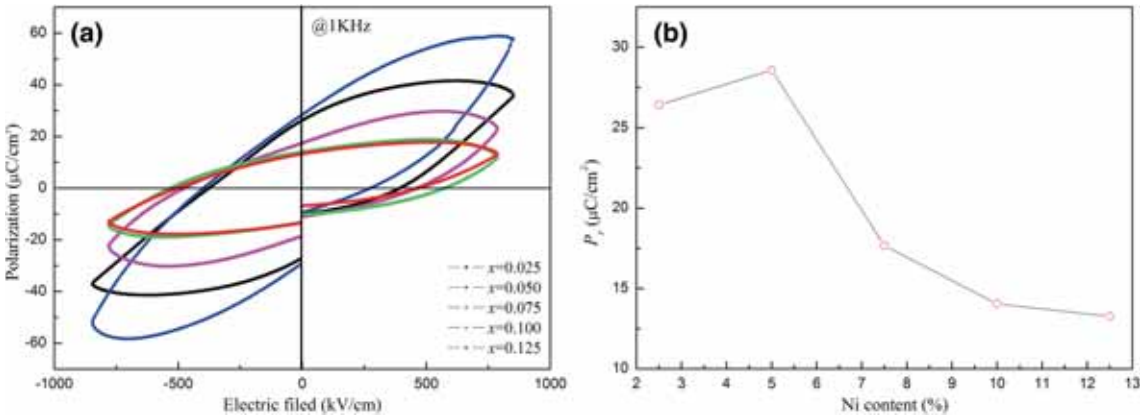

Figure 4. (**a**) P–E hysteresis loops and (**b**) P_r of Au/$Bi_{0.85}Nd_{0.15}Fe_{1-x}Ni_xO_3$/FTO capacitors.

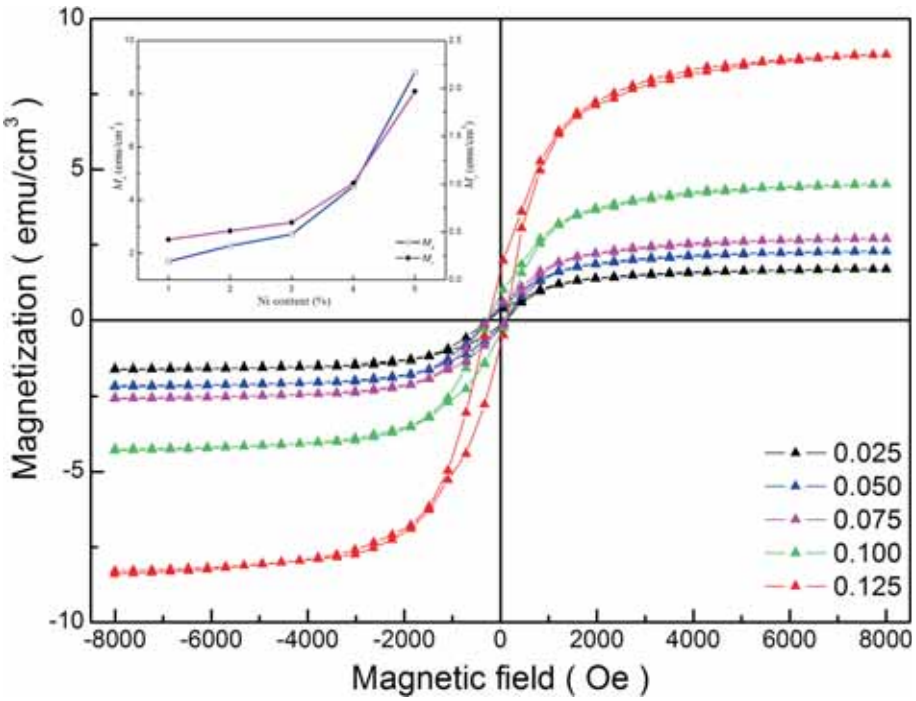

Figure 5. Magnetization hysteresis (M–H) curves of $Bi_{0.85}Nd_{0.15}Fe_{1-x}Ni_xO_3$ thin films (inset shows M_s and M_r).

Figure 5 shows the magnetization hysteresis (M–H) curves of $Bi_{0.85}Nd_{0.15}Fe_{1-x}Ni_xO_3$ thin films with different Ni doping concentrations measured at room temperature, and the inset shows saturation magnetization M_s and remnant magnetization M_r. M_s of $Bi_{0.85}Nd_{0.15}Fe_{1-x}Ni_xO_3$ ($x = 0.025$, 0.050, 0.075, 0.100 and 0.125) thin films at 8000 Oe is 1.69, 2.08, 2.71, 4.52 and 8.81 emu cm^{-3} and M_r of the films is 0.42, 0.51, 0.60, 1.01 and 1.97 emu cm^{-3}, respectively. These results indicate that the saturation magnetization of $Bi_{0.85}Nd_{0.15}Fe_{1-x}Ni_xO_3$ thin films increases with an increase in Ni doping concentration. The ferromagnetism of $Bi_{0.85}Nd_{0.15}Fe_{1-x}Ni_xO_3$ thin films is enhanced with the addition of nickel, which is due to the larger radius of Ni^{2+} than Fe^{3+}. The lattice constant changes when Ni^{2+} enters the lattice of bismuth ferrite, which destroys the original spin cycloid and forms a homogeneous spin structure. The lattice changes release the potential magnetic behaviour.

Figure 6 shows the absorption spectrum and band gap pattern of $Bi_{0.85}Nd_{0.15}Fe_{1-x}Ni_xO_3$ thin films at room temperature. The transmittance of the films is low at 500 nm, which indicates that the absorption rate of the films is large at this wavelength. The transmittance of the films increases with an increase in wavelength. A steep slope appears between 500 and 600 nm and gradually moves to the long wavelength with an increase of Ni dopant content. The existence of this slant shows that the films have obvious intrinsic

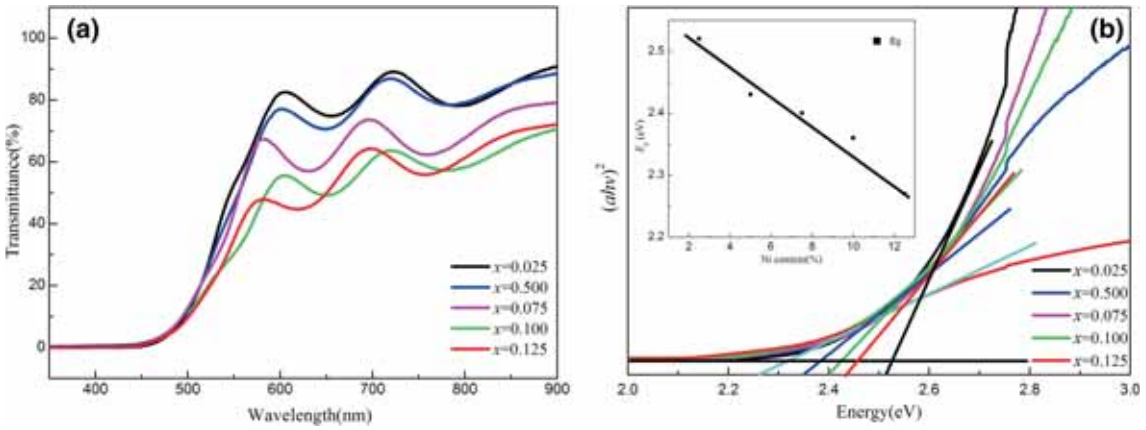

Figure 6. (**a**) Transmittance spectra from 350 to 900 nm and (**b**) $(ahv)^2 \propto hv$ curves of $Bi_{0.85}Nd_{0.15}Fe_{1-x}Ni_xO_3$ thin films.

absorption. As shown in figure 6a, the transmittance of $Bi_{0.85}Nd_{0.15}Fe_{1-x}Ni_xO_3$ thin films in the long wavelength range (>500 nm) is over 85% when x is below 0.05. However, the transmittance of the films decreases with an increase in Ni doping concentration, i.e., the absorption is gradually enhanced. This condition may be due to the introduction of Ni elements, which reduces the oxygen vacancy and Fe^{2+} in the films. Thus, the binding of the defect centres formed by Ni elements is reduced, and the number of free carriers is increased, which result in an increase in long wavelength interval absorption and low transmittance of the films [24]. Figure 6b shows the energy band gap of $Bi_{0.85}Nd_{0.15}Fe_{1-x}Ni_xO_3$ thin films based on $(ahv)^2 \propto hv$, and the inset shows the relationship between the band gap value and Ni dopant content. As shown in the figure, the band gap values of $Bi_{0.85}Nd_{0.15}Fe_{1-x}Ni_xO_3$ thin films decrease with an increase in Ni doping concentration.

4. Conclusions

Ni doping concentration has an important influence on the structure, leakage current, ferroelectric, magnetic and optical properties of $Bi_{0.85}Nd_{0.15}Fe_{1-x}Ni_xO_3$ thin films synthesized through the sol–gel method on FTO substrates. $Bi_{0.85}Nd_{0.15}Fe_{1-x}Ni_xO_3$ thin films are polycrystalline films with a single perovskite structure without any impurity phase when the Ni doping concentration is below 0.1. However, the $Bi_2Fe_4O_9$ phase appears in the sample with an increase in Ni doping concentration. The grain size of the films and their holes gradually decrease with an increase in the Ni doping amount. The saturation magnetization of $Bi_{0.85}Nd_{0.15}Fe_{1-x}Ni_xO_3$ thin films increases with Ni content. However, appropriate Ni doping concentration decreases the leakage current and enhances the ferroelectric polarization and optical transmittance of the films. Meanwhile, the absorption edge of the films is slightly moved to long wave.

Acknowledgements

This work is supported by the Guangxi Experiment Center of Information Science, China (No. YB1416).

References

[1] Fang Y W, Ding H C D, Tong W Y and Duan C G 2014 *Sci. Bull.* **60** 1
[2] Hwang J S, Cho Y J, Park S Y, Yoo Y J, Yoo P S, Lee B W *et al* 2015 *Appl. Phys. Lett.* **106** 062902
[3] Han D, Wang H, Xu J, Yang L and Qiu W 2016 *J. Mater. Sci.: Mater. Electron.* **27** 7501
[4] Wang J, Neaton J B, Zheng H, Nagarajan V, Ogale S B, Liu B *et al* 2003 *Science* **299** 1719
[5] Lebeugle D, Colson D, Forget A, Viret M, Bonville P, Marucco J F *et al* 2007 *Phys. Rev. B* **76** 024116
[6] Das R R, Kim D M, Baek S H, Eom C B, Zavaliche F, Yang S Y *et al* 2006 *Appl. Phys. Lett.* **88** 242904
[7] Wu J G and Wang J 2010 *Acta Mater.* **58** 1688
[8] Yi M L, Wang C B, Shen Q and Zhang L M 2014 *J. Mater. Sci. Mater.: Electron.* **25** 82
[9] Xue X, Tan G, Liu W and Hao H 2014 *J. Alloys Compd.* **604** 57
[10] Rajput S S, Katoch R, Sahoo K K, Sharma G N, Singh S K, Gupta R *et al* 2015 *J. Alloys Compd.* **621** 339
[11] Kim Y J, Kim J W and Kim S S 2013*J. Sol–Gel Sci. Technol.* **66** 38
[12] Han D, Wang H, Xu J, Zhang X and Yang L 2018 *J. Wuhan Univ. Technol. Mater. Sci.* **33** 64
[13] Yan H, Deng H, Ding N, He J, Peng L, Sun L *et al* 2013 *Mater. Lett.* **111** 123
[14] Dong G, Tan G, Luo Y, Liu W, Ren H and Xia A 2014 *Mater. Lett.* **118** 31
[15] Naganuma H, Miura J and Okamura S 2008 *Appl. Phys. Lett.* **93** 052901
[16] Singh S K, Ishiwara H, Sato K and Maruyama K 2007 *J. Appl. Phys.* **102** 094109

[17] Raghavan C M, Kinm J W and Kinm S S 2013 *Ceram. Int.* **39** 3563
[18] Zhang Y L, Yan N, Wang X J, Chen S and Yang S H 2013 *Ferroelectrics* **454** 35
[19] Kumar A and Yadav K L 2011 *J. Phys. Chem. Solids* **72** 1189
[20] Zang X, Sui Y, Wang X, Wang Y and Wang Z 2010*J. Alloys Compd.* **507** 157
[21] Yu B F, Li M Y, Liu J, Guo D Y, Pei L and Zhao X Z 2008 *J. Phys. D: Appl. Phys.* **41** 065003
[22] Singh S K, Maruyama K and Ishiwara H 2007 *Appl. Phys. Lett.* **91** 112913
[23] Liu L, Wang H, Xu J, Yang L and Ren M 2012 *Appl. Mech. Mater.* **110–116** 5483
[24] Pulker H K 1979 *Appl. Opt.* **18** 1969